Local site effects and incremental damage of buildings during the 2016 Central Italy earthquake sequence

Anastasios Sextos,[a)] M.EERI Raffaele De Risi,[a)] Alessandro Pagliaroli,[b)] Sebastiano Foti,[c)] Federico Passeri,[c)] M.EERI Ernesto Ausilio,[d)] Roberto Cairo,[d)] Maria Chiara Capatti,[e)] Filiberto Chiabrando,[f)] Anna Chiaradonna,[g)] Shideh Dashti,[h)] Filomena De Silva,[g)] Francesca Dezi,[i)] Maria Giovanna Durante,[j)] Silvia Giallini,[b)] Giuseppe Lanzo,[k)] Stefania Sica,[l)] Armando L. Simonelli,[l)] Paolo Zimmaro,[j)] M.EERI

ABSTRACT

The Central Italy earthquake sequence initiated on 24 August 2016 with a moment magnitude **M**6.1 event followed by a **M**5.9 and a **M**6.5 earthquake, that caused significant damage and loss of life in the town of Amatrice and other nearby villages and hamlets. The significance of this sequence led to a major international reconnaissance effort to thoroughly examine the effects of this disaster. Specifically,

[a)] Department of Civil Engineering, University of B
[b)] Dipartimento di Ingegneria e Geologia, Universita
[c)] Dipartimento di Ingegneria Strutturale, Edile e Ge
[d)] Dipartimento di Ingegneria Civile, Università dell
[e)] Department of Civil Engineering, University of B
[f)] Dipartimento di Architettura e Design, Politecnicc
[g)] Dipartimento di Ingegneria Civile, Edile e Ambie
[h)] Department of Civil, Environmental & Architectu
[i)] Università degli Studi della Repubblica di San Ma
[j)] Department of Civil and Environmental Engineeri
[k)] Dipartimento di Ingegneria Strutturale e Geotecnica, Sapienza Università di Roma, Italy
[l)] Department of Engineering, Università del Sannio, Italy

this paper presents evidences of strong local site effects (i.e., amplification of seismic waves due to stratigraphic and topographic effects that leads to damage concentration in certain areas). It also examines the damage patterns observed along the entire sequence of events in association with the spatial distribution of ground motion intensity with emphasis on the clearly distinct performance of reinforced concrete and masonry structures under multiple excitations. The paper concludes with a critical assessment of past retrofit measures efficiency and a series of lessons learned as per the behavior of structures to a sequence of strong earthquake events.

INTRODUCTION

Earthquake engineering has a strong theoretical foundation but is also an empirically driven discipline. As a result, post-earthquake reconnaissance efforts provide essential knowledge and help to improve our understanding of seismic events and their effects on the natural and built environment. Post-earthquake reconnaissance reports date back to several centuries ago. A pioneering example is the report by Sarconi dated back to 1784 on the seismic sequence of the year before in Calabria (Italy), in which several illustrations documenting the observed damage and particularly the diffuse liquefaction phenomena were presented.

The 2016 Central Italy seismic sequence caused significant damage and loss of human life with 299 casualties. Three main events occurred between August and October 2016: a **M**6.1 on 24 August, a **M**5.9 on 26 October, and a **M**6.5 on 30 October. Remarkably, the event characterized by the largest magnitude earthquake (**M**6.5, 30 October) occurred when many villages were entirely abandoned following previous events. As a result, although it caused disruption in several villages over a large area, it did not cause any casualty.

After the **M**6.1 event, a joint Italy-UK-USA team conducted a reconnaissance effort under the auspices of the Geotechnical Extreme Events Reconnaissance (GEER) association funded by the U.S. National Science Foundation (NSF), followed by a second reconnaissance mission in October to collect additional data on the cumulative damage of the building stock, earthquake-induced landslides/rockfalls and surface faulting features. GEER (2016; 2017) summarize main findings of both reconnaissance missions. This paper focuses on the observed damage to buildings, its spatial correlation in relation to the intensity of ground motion, including site effects, and the influence of multiple earthquake excitations on the

extent and nature of the damage patterns observed for different structural systems. To serve this purpose, the paper is organized into three main parts as described below.

First, field mission organization, coordination, and activities are presented with emphasis on the methodologies and tools employed. Next, a study of the geological and topographic conditions of the surveyed municipalities and hamlets is presented with the aid of the analysis of a limited number of single station ambient vibration measurements (Horizontal-to-Vertical Spectral Ratio method). Detailed site-response analyses are out of scope for the present study as they are currently in progress within the framework of the seismic microzonation studies that can be found elsewhere (CentroMS, 2016), however, evidences of local site amplification are described within the paper if observed during the surveys.

For three selected towns and villages, namely Accumoli, Amatrice, and Norcia, that were inspected both after the 24 August and the October events, a comparative assessment of quick visual inspections of their entire building portfolio is presented. Where available, a further comparison is made between on-site visual inspections made by the GEER team and the rapid assessment of damage released after each event by means of satellite data (Copernicus, 2016). The paper concludes with the lessons learned in terms of the effect of local soil and site conditions as well as of the cumulative damage caused by the sequence of the earthquake events.

RECONNAISSANCE APPROACH AND METHODOLOGY FOR DATA COLLECTION

To better coordinate the GEER field missions, activities were designed to maximize use of resources and data as they gradually became available. The approach was to combine conventional field reconnaissance activities with advanced imaging and damage detection techniques enabled by information and communications technologies (ICT) and geomatics. A similar multi-scale reconnaissance approach has been implemented by the GEER team to document landslides (Franke et al., 201x – this issue). The steps followed during our reconnaissance effort are described below and illustrated in Figure 1:

Initial planning of the field mission paths: Identification of areas most significantly affected by earthquake-related damage, utilizing available post-event rapid-assessments of damage distribution based on satellite images, released after the earthquake event (Copernicus, 2016; Center for seismic microzonation and its applications – CentroMS, 2016;

Advanced rapid imaging and analysis, ARIA, 2016a). Path optimization was based on: (1) Google Maps information regarding the accessibility of roads and (2) feedback from other GEER groups and local engineers that had visited the area previously.

Use of unmanned aerial vehicles,UAVs (drones): to map areas of affected residential buildings, churches, bridges, landslides and geotechnical systems.

Conventional inspection: on-ground, structure-by-structure visual inspection of buildings and other infrastructures in the selected areas.

Database & GIS: Creation of an *ad-hoc* developed Microsoft Access Database for filling-in the Italian quick inspection form, according to the AeDES guidelines (Baggio, 2007) for post-earthquake assessment of 1313 buildings consistently documented after the 24 August and the October events. Database fields include classification of the structural system, material, soil conditions, damage at a member level between slight (D1), moderate (D2-D3), and very heavy (D4-D5) damage levels and an automated procedure to assign a global damage index for each building based on a weighted average of individual element failures. Conventional hard copy forms were also filled-in for redundancy purposes.

Back-tracking & Documentation: A unique ID was assigned to each building along with the coordinates associated with a waypoint (path tracked with handheld GPS) for easy back-verification of position to each building. Storage of the geo-tagged photos taken on-site in the database matched with complementary pre-earthquake photos retrieved by Google Street View

GIS: Development GIS shapefiles containing the surveyed buildings footprints and the associated data from the database to visualize the spatial distribution of structural damage.

Manual completion: Population of the missing data for approximately 20% of the buildings for which detailed on-site visual inspection was not feasible due to accessibility issues, based on the existing photos, pre-quake and satellite images, drone footage (Sextos, 2016), and engineering judgment.

Validation of satellite-based quick damage assessment: Database validation to ensure that the observed damage was solely the result of earthquake excitation and not of any post-earthquake intervention (i.e. post-earthquake controlled-demolitions), through comparison with of the observed damage with Copernicus images that were taken closer to the event.

Effect of multiple earthquake events: Quantification of the damage evolution after multiple seismic events for different structural systems, i.e., reinforced concrete and masonry buildings.

Correlation to ground motion intensity measures (IMs) and site effects recognition: Correlation, where possible, of the observed damage with mapped geological information and preliminary analysis of the influence of site effect on structural damage patterns utilizing rapid non-invasive *in-situ* investigation based on single station ambient vibration measurements (HVSR method).

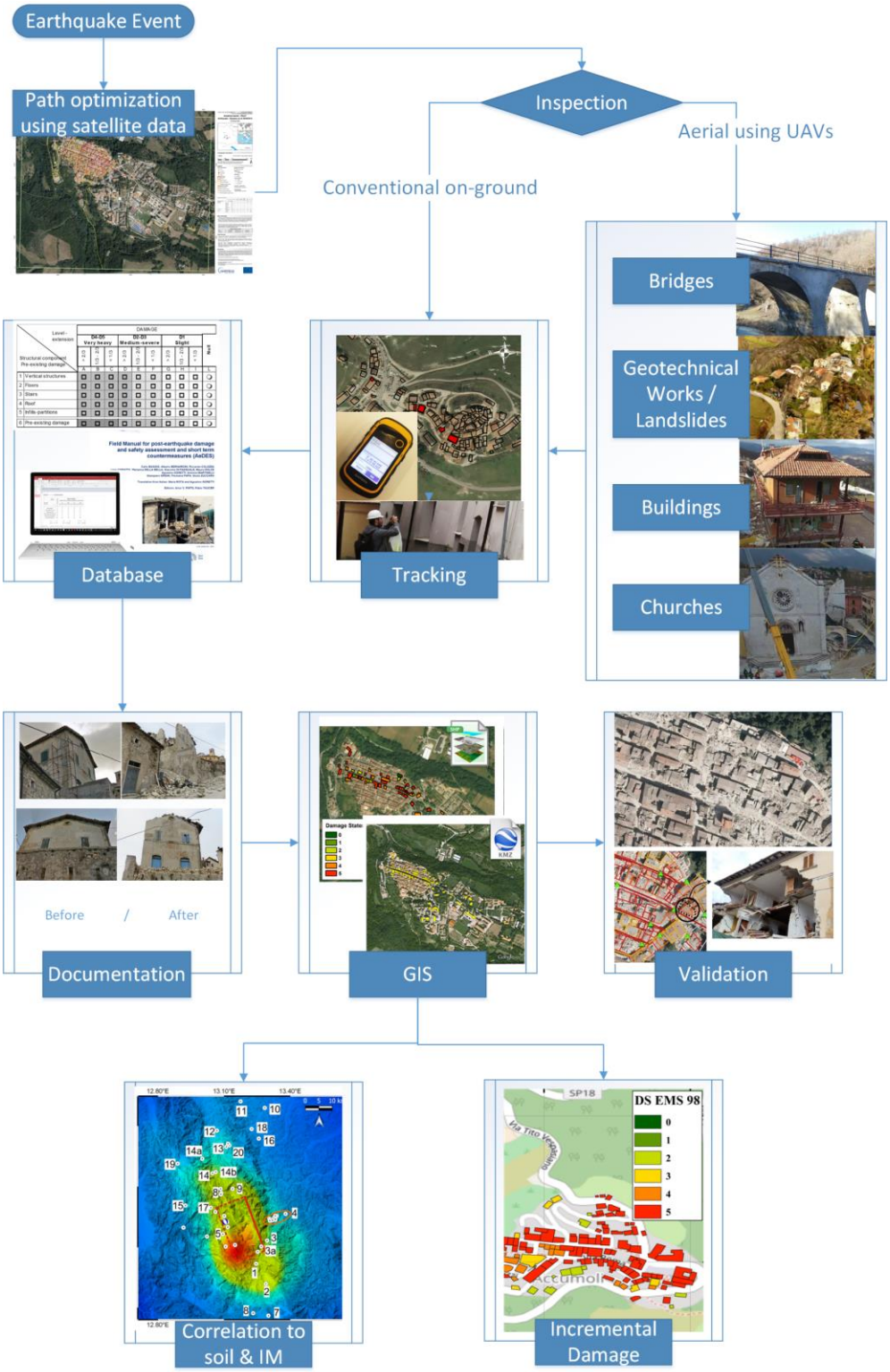

Figure 1. Overview of the reconnaissance strategy and organization.

SEISMIC SITE EFFECTS ON DAMAGE PATTERNS

Seismic site effects are usually associated with: (a) local ground response (also referred to as stratigraphic effect), (b) topographic amplification/deamplificaton, or (c) basin/edge

effects. These phenomena are widely recognized in the literature (Roesset, 1970; Sanchez-Sesma, 1987; Seed et al., 1988; Frankel and Vidale, 1992; Olsen and Schuster, 1995).

Local ground response (i.e., stratigraphic effect) is mainly due to seismic wave propagation within near-surface soil deposits, where significant variations in amplitude, frequency content, and duration occur (e.g., Faccioli et al. 2002, Pagliaroli et al. 2011) as a result of stratigraphic and buried morphology features. Similarly, amplification of seismic waves due to topographic irregularities is an important cause of damage localization during seismic events (e.g., Bard and Riepl-Thomas 2000) as documented by several studies in Italy (Brambati et al. 1980, Siro 1982, Rovelli et al. 1998, Marsan et al. 2000, Paolucci 2002) and worldwide.

According to the Italian building code (Ministry of Infrastructure, 2008; hereafter NTC 2008), these effects on ground motion are accounted for by multiplying the reference ground motion at the site with a deterministic amplification factor. The latter is derived from simplified classification parameters that are related respectively to: the averaged shear wave velocity of the upper 30m ($V_{S,30}$), as per Eurocode 8 (CEN 2004, clause 3.1.2); shape of the site and slope inclination for topographic effects. This procedure is usually referred to as hybrid approach (Cramer, 2003). However, the combination of probabilistic hazard models with deterministic amplification factors, produce results that are biased in terms of medians and ground motion variabilities and do not preserve the target hazard level in the modified ground motion level (Gallipoli et al. 2013, Stewart et al. 2014, Stewart et al. 2017). Furthermore, comparisons between the hybrid approach and a more robust non-ergodic procedure (in which the effects of site amplifications are included within the hazard calculation) show that the former method tends to underestimate ground-shaking levels (i.e., Goulet and Stewart 2009, Zimmaro et al., 2017).

To evaluate the spatial distribution of ground motion intensity measures during the studied sequence of earthquake events, Zimmaro et al. (201x, this issue) applied a Kriging procedure to within-event residuals (i.e. the difference between recorded and estimated ground motions using global ground motion models, for a specific earthquake event) for uniform reference site-conditions of $V_{S,30}$=580 m/s (considered site class B according to NTC 2008) that were deemed representative of this region. The first step of this approach is to calculate within-event residuals at all recording station sites, using the average of the following Italy-adjusted global ground motion models: Boore et al. (2014), Campbell and

Bozorgnia (2014), and Chiou and Youngs (2014). Then, the spatial distribution of a given intensity measure is estimated using the Jayaram and Baker (2009) global correlation model (i.e. a semi-variogram that describes the spatial variability of a given ground motion intensity measure throughout the area). All source-to-site distance were calculated using trimmed finite fault models presented in Galadini et al. (201x, this issue). The Italy-specific regional adjustment adopted in these models is needed to capture a relatively steep ground motion attenuation with distance observed in Italian events (e.g. Stewart et al., 2012). The effectiveness of the adoption of global models with region-specific adjustments for ground motion characterization studies in Italy, has been recently illustrated by Zimmaro and Stewart (2017). Further details on the approach used to estimate the ground motion are provided in GEER (2017) and Zimmaro et al. (201x, this issue). Following this approach, ground motion intensity estimations for the three main shocks were obtained for a grid of sites in the epicentral area, as well as for hamlets, towns, and cities for which co-located recording instruments were not available (i.e. where no recording stations were available or they did not record the events).

Figure 2 shows the spatial distribution of peak ground acceleration (PGA) for the three main shocks. In Table S1, a summary of PGA values for visited locations along with a detailed analysis of site-specific geological conditions is also provided. Main municipalities and hamlets covered in this paper are labeled in Figure 2, with a sequence number consistent with those reported in Table S1. It is important to note that the contour map showing spatial distribution of PGA shown in Figure 2 and the PGA values at selected locations summarized in Table S1, do not properly account for local effects since uniform generic site conditions were assumed for the entire area. Furthermore, each damage level value in Table S1 represents an average damage level in the villages, while intra-village damage patterns are discussed in a subsequent section.

The estimated values of PGA at each inspected village are compared in Table S1 with the average damage level documented during the reconnaissance. The damage was classified on the basis of visual inspections of buildings following the scheme provided by the Department of Civil Protection (DPC) in Italy for post-earthquake reconnaissance purposes. As shown in Table 1, the damage scale ranges from D0 which denotes “no observed damage” to D5 that corresponds to collapse (EMS 98, Grunthal, 1998; Bray and Stewart, 2000). Moreover,

synthetic descriptions of topographic features of each visited municipality are reported in Table S1.

In the following section, selected examples of local site effects at several locations are shown. The main goal is to identify if structures that can be considered homogeneous and therefore equally vulnerable (i.e., same age, structural system, etc.) have been affected in different manner by the specific site conditions with respect the final observed damage. Therefore, the following observations are intended to highlight only the effects of ground motion spatial variability across villages due to specific stratigraphic and topographic configurations. Incremental structural damage assessment after different shocks is presented later.

Montegallo

Montegallo is a village composed of 23 small hamlets spread over a large area. It is characterized by an altitude varying significantly from the hamlet of Uscerno (i.e., 494m A.S.L.) to the highest peak of Colleluce at 1023m.

Table 1. Definition of damage classification (adapted from Bray and Stewart, 2000).

Damage Level	Description	Tag Color
D0	No Damage	
D1	Cracking of non-structural elements, such as dry walls, brick or stucco external cladding	
D2	Major damage to the non-structural elements, such as collapse of a whole masonry infill wall; minor damage to load-bearing elements	
D3	Significant damage to loading-bearing elements, but no collapse	
D4	Partial structural collapse (individual floor or portion of building)	
D5	Full collapse	

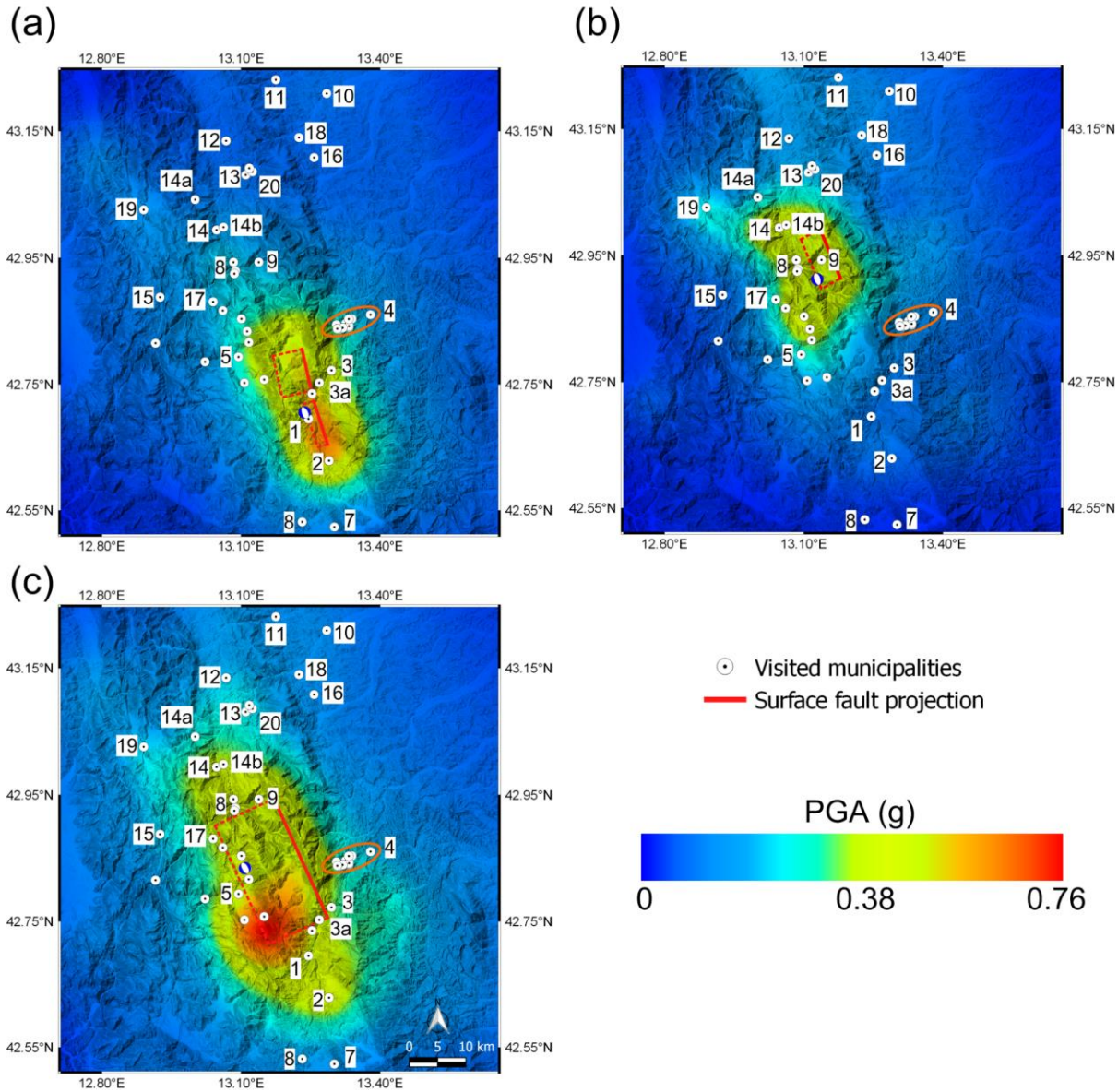

Figure 2. Location of visited municipalities and hamlets, epicenter locations (moment tensors), and spatial distribution of PGA for the: (a) 24 August **M**6.1, (b) 26 October **M**5.9, and (c) 30 October **M**6.5 earthquakes. Numbers in Figure 2 are those presented in Table S1.

The geology of Montegallo is characterized by eluvial-colluvial deposits consisting of silty sand and mixtures of silt and sand, as well as alluvial terraced deposits (Figure S1). The bedrock is a turbiditic succession known as Laga Flysch mainly composed of arenaceous and arenaceous-pelitic lithofacies. However, specific geologic-topographic characteristics widely vary across the area, leading to a significant heterogeneity in damage patterns even for buildings with apparently similar structural type and vulnerability.

An evidence for ground shaking variability is the undamaged hamlet of Piano in the NNE area of Montegallo. Despite examples of poorly constructed masonry buildings, there was no

sign of evident damage at the end of the seismic sequence. For Piano, it is expected the absence of stratigraphic amplification given the visible outcropping rock in this area (Figure 3-P01). A second example is a slight damage (i.e., D0-D2) observed in the hamlet of Pistrino di Sotto (Figure 3-P02), which is less than 500m away from Piano, on the opposite side of the NNE hill. It is also arguable that Pistrino di Sotto is resting on shallow bedrock conditions. These geologic conditions, combined with the relatively high natural frequency of the site, likely did not produce significant amplification of the ground motion. On the contrary, the adjacent hamlet, Pistrino di Sopra (Figure 3-P03), presented a significant level of damage, most likely associated with the presence of a soft cover of elluvial-colluvial deposits. These conditions are typical of the area, as shown in Figure S1.

Other Montegallo's hamlets, such as Astorara, Castro, and Colleluce in the southwestern part of the area at a distance of 1.5 to 2.5km from Piano, located on quaternary deposits resting on rock, experienced high levels of damage and several cases of total collapse (D5). For example, Figure 3-P04 shows a street in Castro that was blocked by the debris of a damaged building. Given the proximity between Castro (highly damaged) and Piano (practically undamaged), and the very similar structural systems and construction standards, it is probable that Castro experienced stronger ground motions than Piano, due to significant topographic amplification. A view of the 3D model obtained with a drone survey over the entire area can also be found in BYU-PRISM (2016). It shows the typical crest configuration of the zone, leading to possible 2D topographical effects.

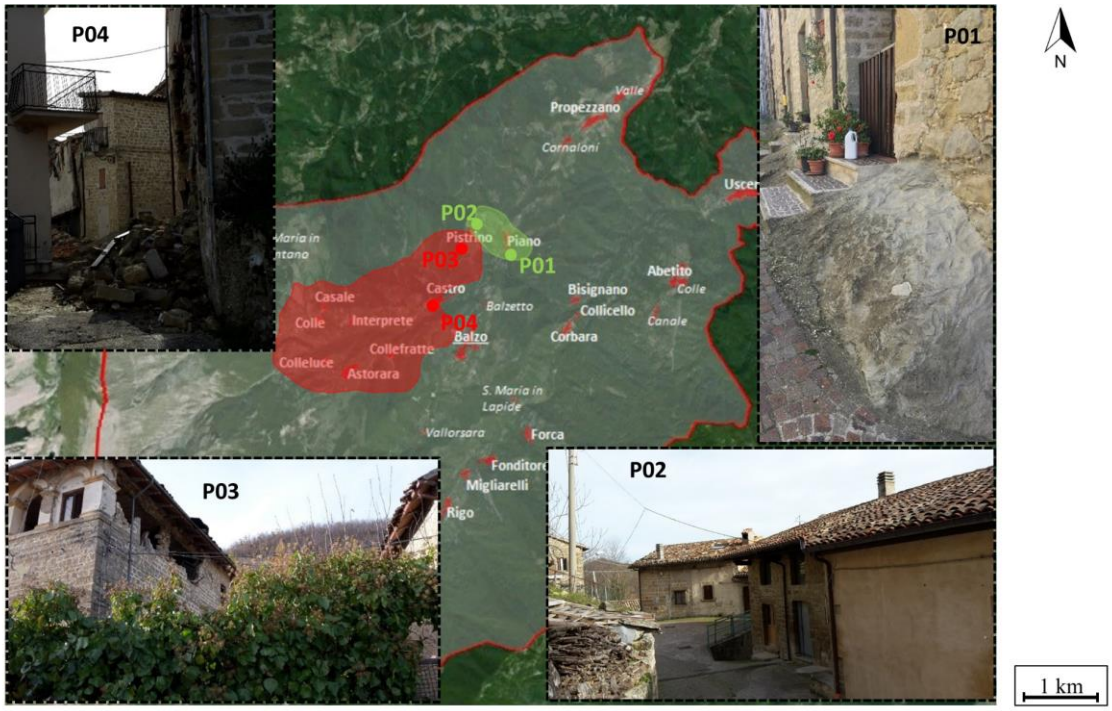

Figure 3. Spatial distribution of building damage across the municipality of Montegallo.

San Severino Marche

Other examples of local site effects were identified in some areas of San Severino Marche (number 11 in Figure 2). San Severino Marche is a town in the Province of Macerata, in the Marche region, located about 50 kilometers south-west of Ancona and about 25 kilometers south-west of Macerata. It has about 12,000 inhabitants, and it comprises more than 40 hamlets. Unlike Montegallo, San Severino has districts where most of the buildings are of reinforced concrete, built in the 1960s and the 1970s. Within San Severino Marche, two neighborhoods along Via Mazzini and Via Rossini attracted most of the GEER reconnaissance team attention due to the evident and quite localized damage observed (Figure 4). Via Mazzini is located uphill while buildings along Via Rossini are constructed on the ancient riverbed of the Potenza River. It is deemed that stratigraphic amplification is likely to have taken place due to the presence of soft shallow sediments resulted from the river artificial channeling operations. Similar damage patterns and site effects have been observed in Tolentino (number 10 in Figure 2), as described in GEER (2017).

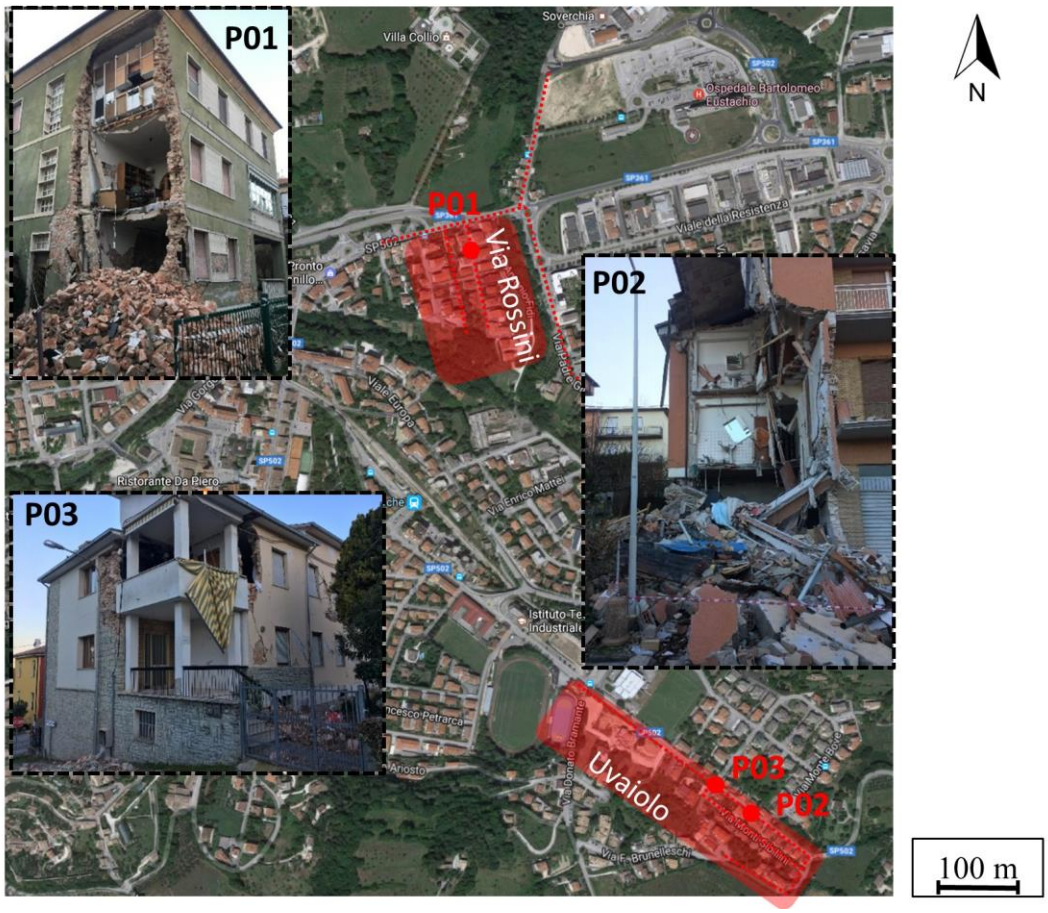

Figure 4. Characteristic building damage within the town of San Severino Marche.

Fiume

Fiume is a hamlet in the province of Macerata (Marche region) and is approximately 4 kilometers away from the town of Pieve Torina. An extract from the 1:10.000 geological map is given in Figure S2. The geologic bedrock of the area of interest is characterized by Scaglia Cinerea, a grey marly limestone (SCC). The western part of the hamlet of Fiume is built on Holocene travertine, travertine plaques and calcium carbonate-encrusted (MUSf1), i.e., materials that are typically tender and crumbly. On the contrary, the Eastern part of the village is built on softer deposits constituted by Holocene eluvial-colluvial deposits (MUSb2), recent alluvial deposits, mainly made of silts and sandy clay intercalated with marl and limestone (MUSb) and debris flow deposits, mainly limestone debris and gravels with a silty-sandy matrix (MUSa).

The Fiume building stock consists mainly of low-rise unreinforced masonry structures, some of which retrofitted to some extent. Locations and pictures of representative structures inspected in Fiume are reported in Figure 5 illustrating the severe and extensive damage. Notably, the degree of damage to buildings was highly variable across the village. The

eastern part of the hamlet, founded on colluvial and alluvial deposits resting on bedrock, suffered high levels of damage (D3) as shown in reference pictures P01-P02-P04, whereas the western part, built on travertine rock, had only negligible damage (D0/D1, P03).

Two noise measurements (T01-T02 in Figure 5) were performed in the damaged zone (east side of the hamlet) during the GEER mission. A portable Tromino tomograph was employed and the total duration of each measurement was approximately 15 minutes. Horizontal-to-Vertical (H/V) spectral ratios were computed by using the geometrical mean of horizontal components. In addition, H/V ratios were computed by rotating the horizontal component between 0° and 180° (directional or polar HVSR), in order to investigate preferential directions of site amplification (i.e., the polarization of ground motion). Both H/V and polar H/V are reported in Figure 5 showing a large H/V peak around 4 Hz, which shows significant stiffness contrast between the upper soil layers and the underlying bedrock, i.e. a typical proxy of local site amplification.

Visso

Located in a valley 607m A.S.L. and surrounded by mountains of the National Park of Monti Sibillini, Visso is a municipality in the Marche region with a population of 1,100 people living in 13 hamlets covering a wide area of approximately 100km^2. The geological setting of the area is shown in Figure S4. The outcropping formations belong to the Cretaceous Miocene basinal succession made of, from bottom to top, Scaglia Rossa Fmt (SAA), Scaglia Variegata Fmt (VAS) and Scaglia Cinerea Fmt (SCC), Bisciaro Fmt (BIS). They are organized in a monoclinal architecture striking from NNW-SSE to N-S, and dipping to W with low-to-moderate angles and crossed by normal fault systems, mainly striking NW-SE. From a morphological viewpoint, Visso is located in a depressed area of the Sibillini Mountains, driven by quaternary normal faults, where the basinal successions are covered by quaternary alluvial and eluvio-colluvial sediments, and widespread slope deposits. The thickness of the covering layer varies from few meters to 40m, reached below the more recent urbanized area of Visso (Figure S4).

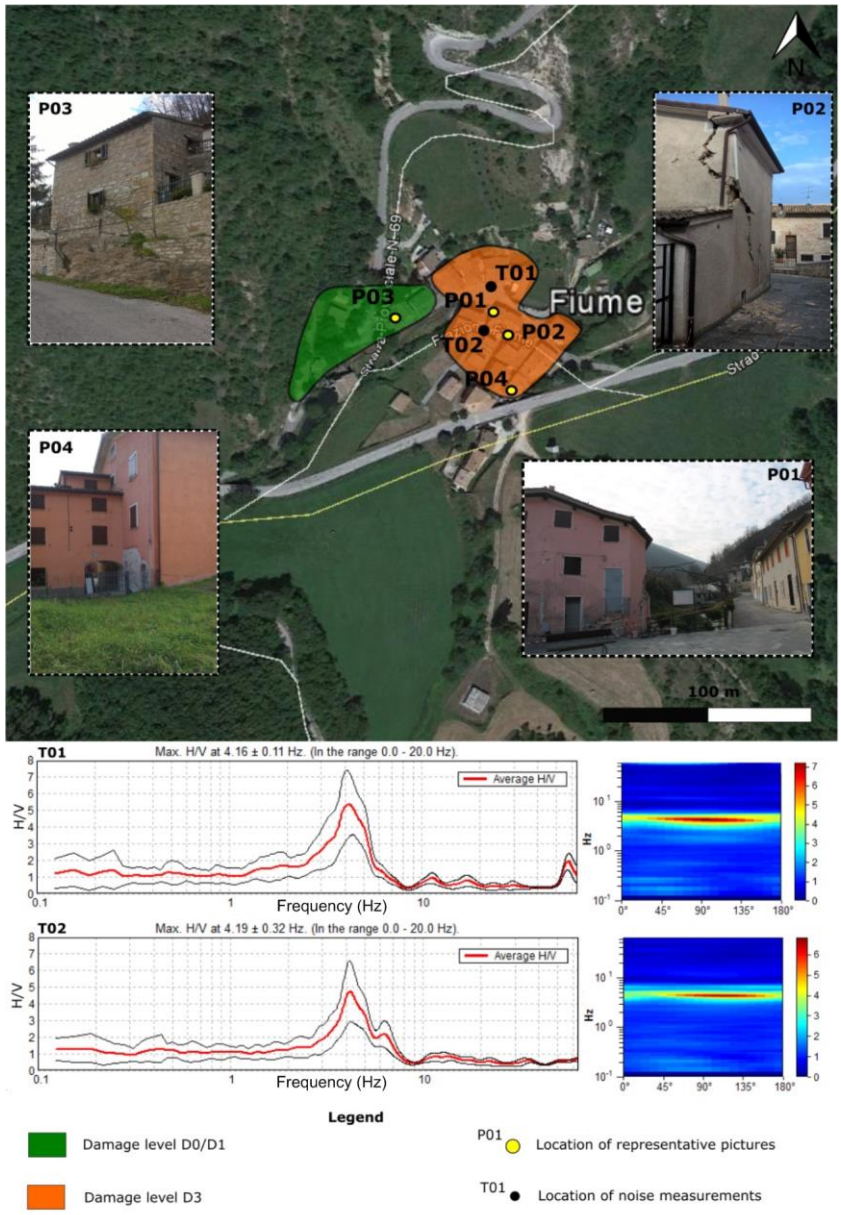

Figure 5. Damage zonation within the village of Fiume (up). Location and results of noise measurements in terms of H/V spectral ratio (bottom left) and polar plot (bottom right).

Most of the buildings in Visso are unreinforced masonry structures, while a limited number of reinforced concrete buildings is also present. These structures are mainly 2 to 3 stories, mostly built before the 1920s. The damage distribution, detected during the GEER site-inspection after the **M**6.5 30 October event, is superimposed on the geological map in Figure S4. As expected, buildings with most damage were 2 to 3 stories, unreinforced masonry structures (sometimes recently retrofitted), mainly located in the historical center (red line in Figure 10). Site amplification effects likely occurred, since most damage (level

D3-D4) was concentrated in the buildings founded on the quaternary continental deposits, while minor damage (level D1-D2) occurred in the portion founded on the SCC rock.

As anticipated, better performance (D2-D3) was detected for the reinforced concrete structures outside the historical center, despite their placement on the quaternary deposits, an observation that is in line with the detailed building-by-building inspection of other towns described in the following sections.

Camerino

Camerino is a village with 43 hamlets of about 6,986 inhabitants, located in the province of Macerata. The reconnaissance activity focused on the historic center where almost 50 buildings were inspected.

The bedrock in the area consists of a typical alternation of arenaceous and pelithic-arenaceous lithofacies (ALS), sometimes with clayey-calcareous marl (COS), called “Scaglia cinerea” and “Schlier”. The above formations are locally covered by eluvio-colluvial soils (ML in Figure S5), made of silt or low-plasticity clay, or alluvial soil (GM) in the valley. The historic center is placed on the above layered arenaceous formation (GRS) referred to as “Formazione delle Arenarie di Camerino” (blue zones) (Figure S5). Where the bedrock is covered by thin layers of eluvio-colluvial soils (ML), ground motion amplification may be expected due to the high impedance contrast.

Figure 6 depicts the damage distribution across the main village, as inspected after the 30 October event. Relatively low damage (D0 or D1) were observed within the inner part of the ridge characterized by local bedrock (GRS) outcrops. Higher damage levels (D2-D3) were observed for many of the low rise (2-3 stories) unreinforced masonry buildings, even if some of them were partially retrofitted. The damage is mainly localized on the hillside, where potential topographic amplifications and permanent deformation (due to slope instability) may be occurred. The highest damage level (D4) was observed at the SW side of the historic center and at the bottom of the Camerino hill, where several masonry structures collapsed. The observed damage distribution pattern in Camerino is consistent with site effects that could be inferred from the geological map shown in Figure S5. Strong amplification of earthquake ground motions is highly probable given the thin soft layers of eluvio-colluvial soils (ML) overlying the bedrock.

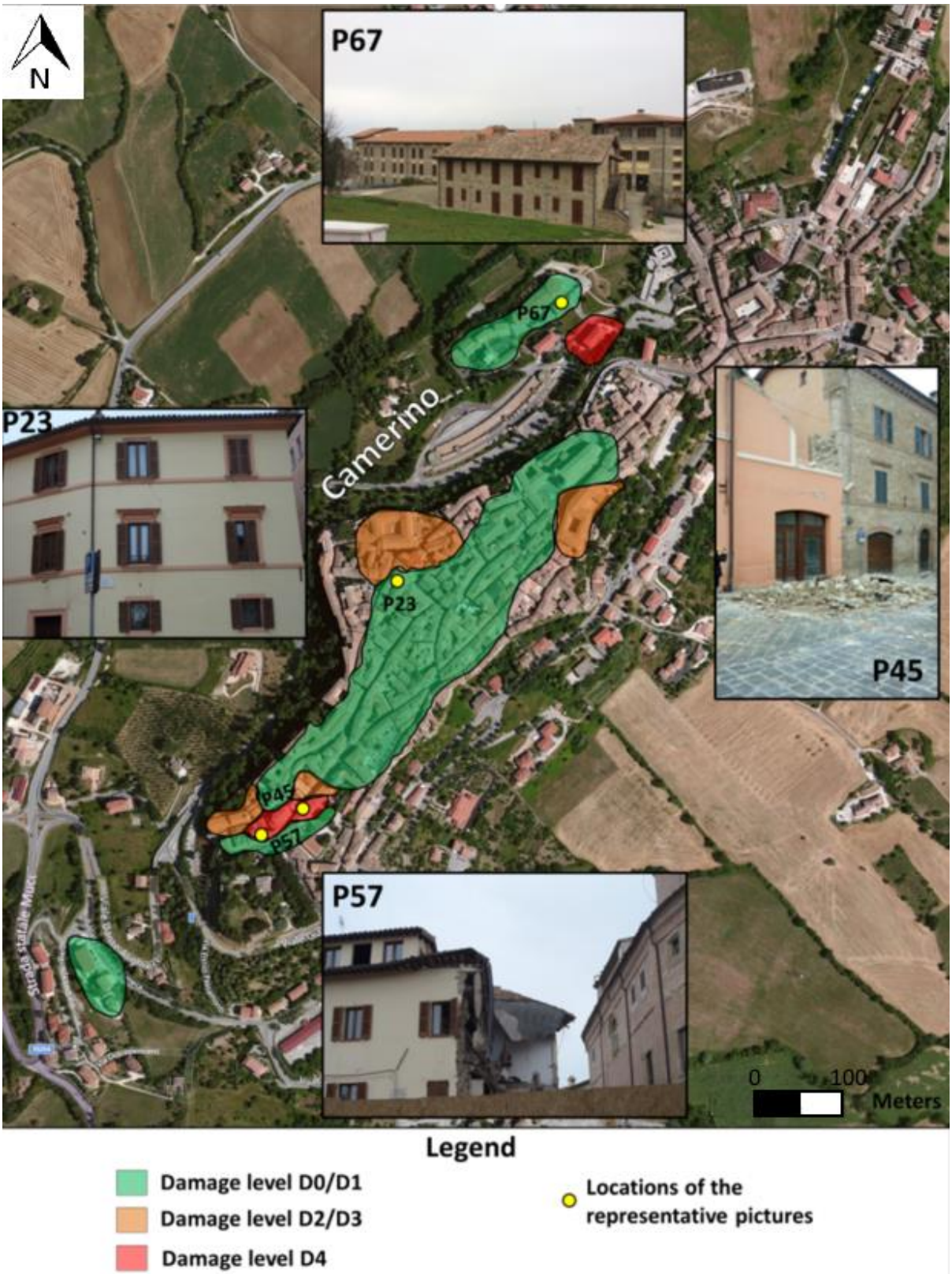

Figure 6. Damage zonation within the historic center of Camerino with pictures of the representative structures inspected.

INCREMENTAL STRUCTURAL DAMAGE

An effort was also made to study the performance and incremental damage of different structural systems under the entire sequence of the August and October events. To this aim, an almost complete building-by-building inspection was performed, after the first and the third mainshocks, in three municipalities: Accumoli, Norcia, and Amatrice.

Accumoli

Soil conditions and building stock

Accumoli is a small municipality in the Lazio region composed of seventeen hamlets covering an area of about 87.3 km^2, with a population of about 670 inhabitants. The main village, which was one of the main targets of the surveys, is located on a steep slope of a ridge elongated in the direction WNW-ESE, with an altitude spanning between 810 and 890 meters above the sea level. According to the 1:500,000 Italian geological map (Ministry of the environment, 2014), the geological bedrock is made of sedimentary lithology units composed of sandstones and clay lithofacies of the late Miocene. The vast majority of the entire building portfolio is composed of masonry residential buildings, with just a few reinforced concrete buildings. Approximately 8% of buildings are one-story, 42% are two-story, 43% three-story, and the remaining 7% are four-story or higher. According to the latest 2011 census survey (ISTAT, 2011), 23%, 68% and 9% of the buildings were identified in an optimum, good, or acceptable conservation status, respectively. Most of these buildings (59%) were constructed before 1919, 32% between 1919 and 1945, 6% between 1946 and 1960, 1% between 1961-70, 1% between 1971-80, and finally 2% between 1981-90.

Incremental damage observed

Figure 7 illustrates the structural damage levels observed during the two surveys, after the 24 August (left) and the October events (right). After the August 24t event, the most severe damage was observed at the eastern side of the village, while the vast majority of the building stock retained its structural integrity null or with minor damage (D0-D1). However, at the end of the seismic sequence, Accumoli was almost completely destroyed. Few buildings, in the south end of the village survived the sequence of events with limited damage (D2).

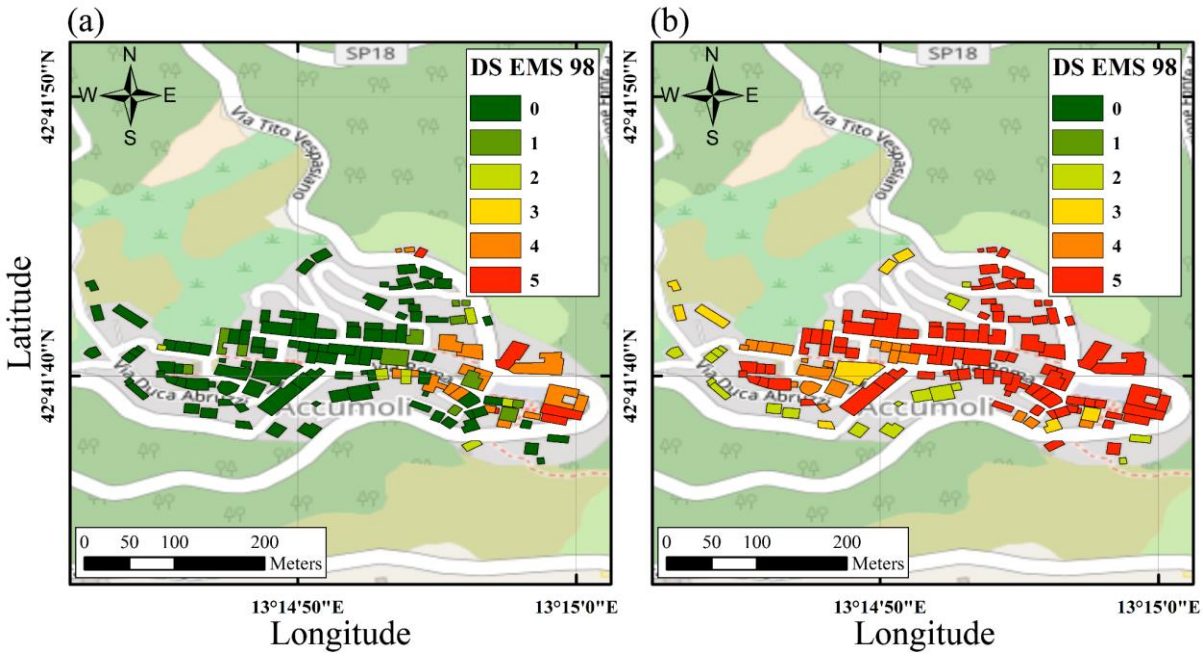

Figure 7. Damage levels in the main village of Accumoli (a) after the first earthquake and (b) at the end of the entire sequence.

The evolution of structural damage during the earthquake sequence is clearly reflected in the observed damage: 72% of the buildings experienced zero (DS0) and 8% minor damage (DS1) after the first earthquake, while not a single building was found intact or with minor damage after the seismic sequence. Large damage states were in contrast more populated (4% to 13% for DS2, 0% to 7% for DS3, 12% to 14% for DS4, and a major shift from 4% to 65% for DS5).

Figures 8a and 8b show an aerial view of the east part of the village during the first and the second surveys, respectively, including the local church and the police station, which eventually collapsed because of multiple earthquake excitations. Figures 9, 10 and 11 illustrate characteristic cases of minor-to-moderate shear and out-of-plane damage after the August event that led to abrupt collapse because of the earthquake sequence. Age of construction, high spectral accelerations for periods lower than 0.3s (which match the natural periods of low-rise buildings) and the variation of spectral polarization across several events were likely the main contributors to the observed catastrophic damage patterns. Given the location of Accumoli, topographic effects may also have contributed to the observed damage.

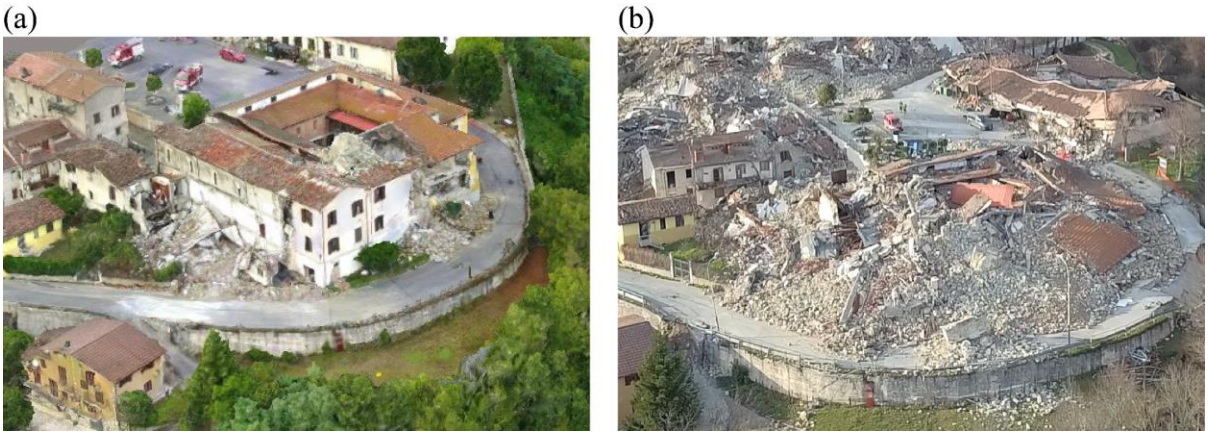

Figure 8. Aerial photos of the east side of Accumoli after (a) the first earthquake and (b) the entire earthquake sequence.

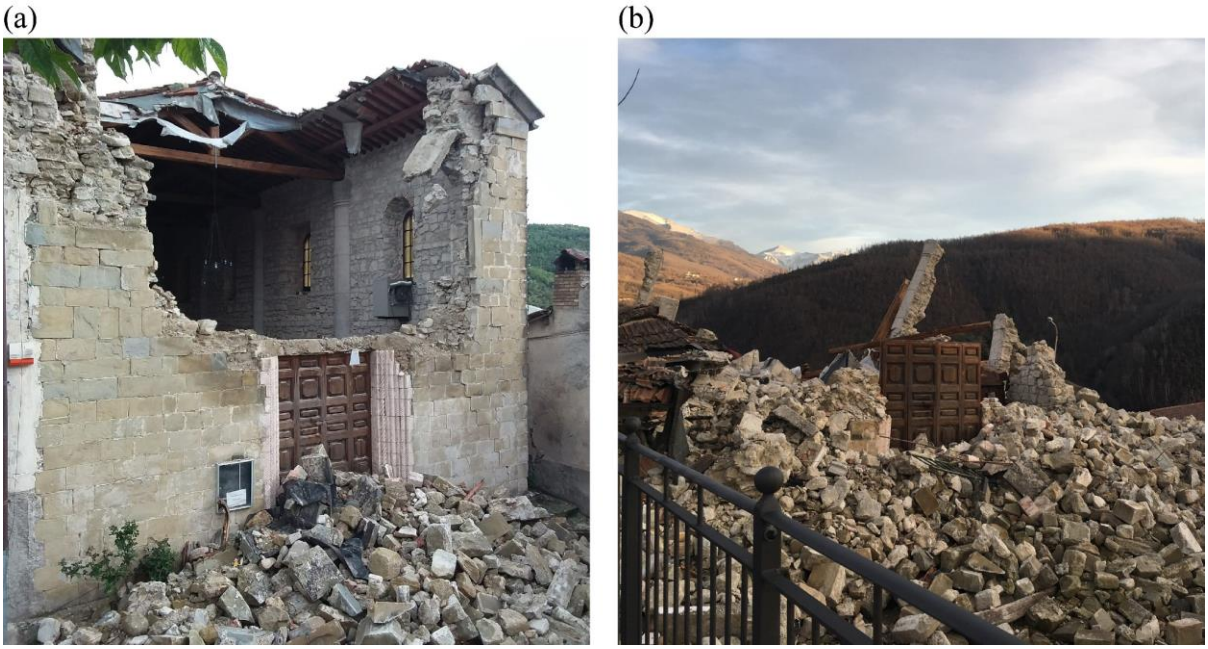

Figure 9. The local church: (a) after the first earthquake; and (b) after the entire sequence.

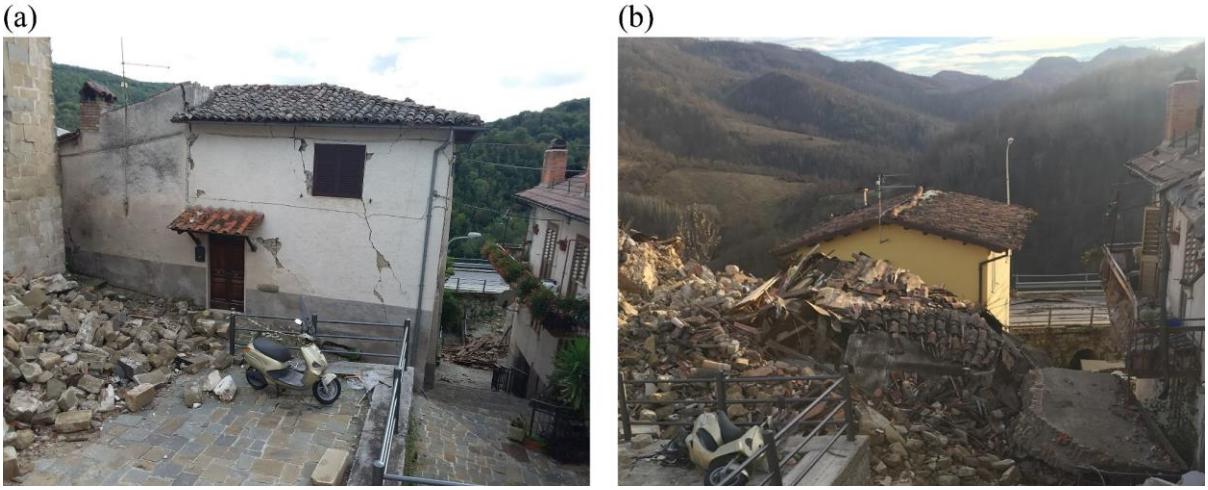

Figure 10. Masonry residential building: (a) after the first earthquake; and (b) after the sequence.

Figure 11. The town hall: (a) after the first earthquake; and (b) after the entire sequence.

Amatrice

Soil conditions and building stock

Amatrice is a municipality in the Lazio region. It is composed of forty-nine hamlets covering an area of about 174.4 km^2, with a population of about 2,630 inhabitants. The town is located on the edge of a hill, with an altitude spanning between 925 and 950 meters. The soil conditions in the area of Amatrice consist of sedimentary lithology units, sandstones and clay lithofacies of the late Miocene. The total number of the buildings inspected over the two field missions was 491, 77% of which were masonry structures for residential purposes. The remaining 11% and 13% are made of reinforced concrete and other structural typologies (i.e., steel, timber, etc.), respectively. Most of the buildings are two stories (48%), while 41% are three-story, 8% one story and the remaining 5% four-stories or higher. According to the latest 2011 census survey (ISTAT, 2011), the 29%, 53%, 14%, and the 3% of the buildings were assessed having an optimum, good, acceptable, and unacceptable conservation status, respectively. The distribution of the building age is as follows: 22% were built before 1919, 24% in between 1919-1945, 13% between 1946-60, 23% between 1961-70, 11% between 1971-80, 4% between 1981-90, 3% between 1990 and 2000, and only 1% after 2005. Hence only about 4% of the entire stock was designed complying with modern seismic codes.

Incremental damage observed

Figure 12 shows the structural damage levels observed during the two surveys. The 24 August event caused severe damage to the south-east part of the historical city center along the main avenue (Corso Umberto I). As observed in the case of Accumoli, many buildings that were still standing after the first event with only a small residual capacity to additional horizontal actions, fully collapsed because of the subsequent September and October events. The shifting of damage states between the aftermath of the first event and the end of the

entire sequence is reflected in the following inspection results clearly indicating a major shift to most critical damage states: intact buildings (D0) were reduced from 30% to 18%, buildings with minor damage (D1) were increased from 5% to 10%, moderate damage (D2) was reduced from 24% to 6%, D3 increased from 1% to 21%, D4 decreased from 17% to 3%, and collapsed buildings (D5) had a significant increase from 23% to 42%.

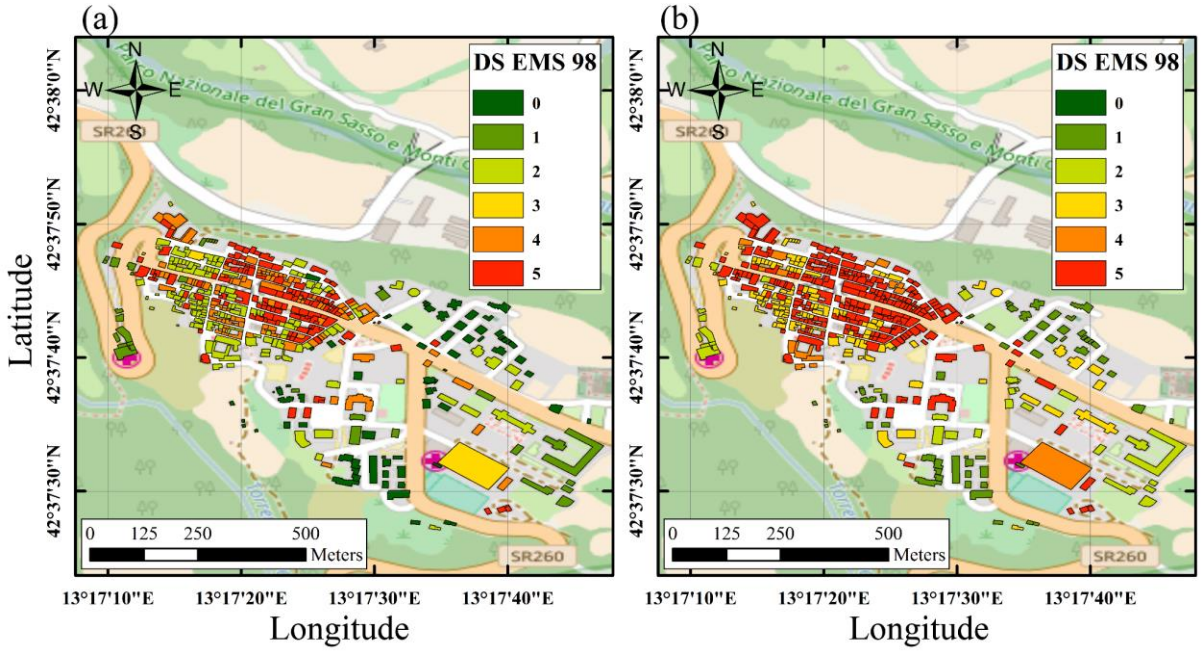

Figure 12. Damage levels observed in the center of Amatrice (a) after the 24 August earthquake (during the first survey), and (b) after the entire sequence (during the second survey).

Even though the statistical sample of the reinforced concrete buildings was not adequate to quantify how damage accumulates for different structural systems under multiple earthquakes, an effort was made to compare characteristic cases at least qualitatively. An example of a reinforced concrete building is illustrated in Figure 13. The partial out-of-plane collapse of an external infill panel after the first event was followed by complete failure at the end of the entire seismic sequence. A closer inspection of the top right beam-column joint further reveals shear damage that was magnified, though not considerably, under multiple excitations, i.e. the reinforced concrete structure retained some of its capacity thus avoiding collapse. A similar example is shown in Figure 14. Cyclic degradation, concrete spalling and minor longitudinal rebar buckling were indeed observed in the absence of adequate transverse reinforcement, however, global damage state remained constantly moderate despite the multiple earthquake events. In some cases, damage accumulation was more significant, as for instance, in the building depicted in Figure 15, where minor damage after

the 24 August event propagated to the major out-of-plane failure of the majority of its infill panels, plastic hinge formations at the end of the exposed column and a degree of residual drift. However, the collapse was prevented. To the Authors' best knowledge, only one reinforced concrete building in Amatrice that was damaged by the 24 August earthquake eventually collapsed in the aftermath of the 26 October event. This structure was a seven-story building with external red curtain walls. More details about the performance and the exact location of this building are discussed in GEER (2017). An interesting case of a multi-story building that survived the multiple seismic excitations within Amatrice's historical center, is a steel structure (Figure 16) built in the early 90's following the 1996 Italian seismic code (Ministry of Public Works, 1996).

Figure 13. Reinforced concrete residential building (a,c) after the 24 August earthquake and (b,d) after the entire sequence. (a,b) External infill failure and (c,d) shear failure at the column top.

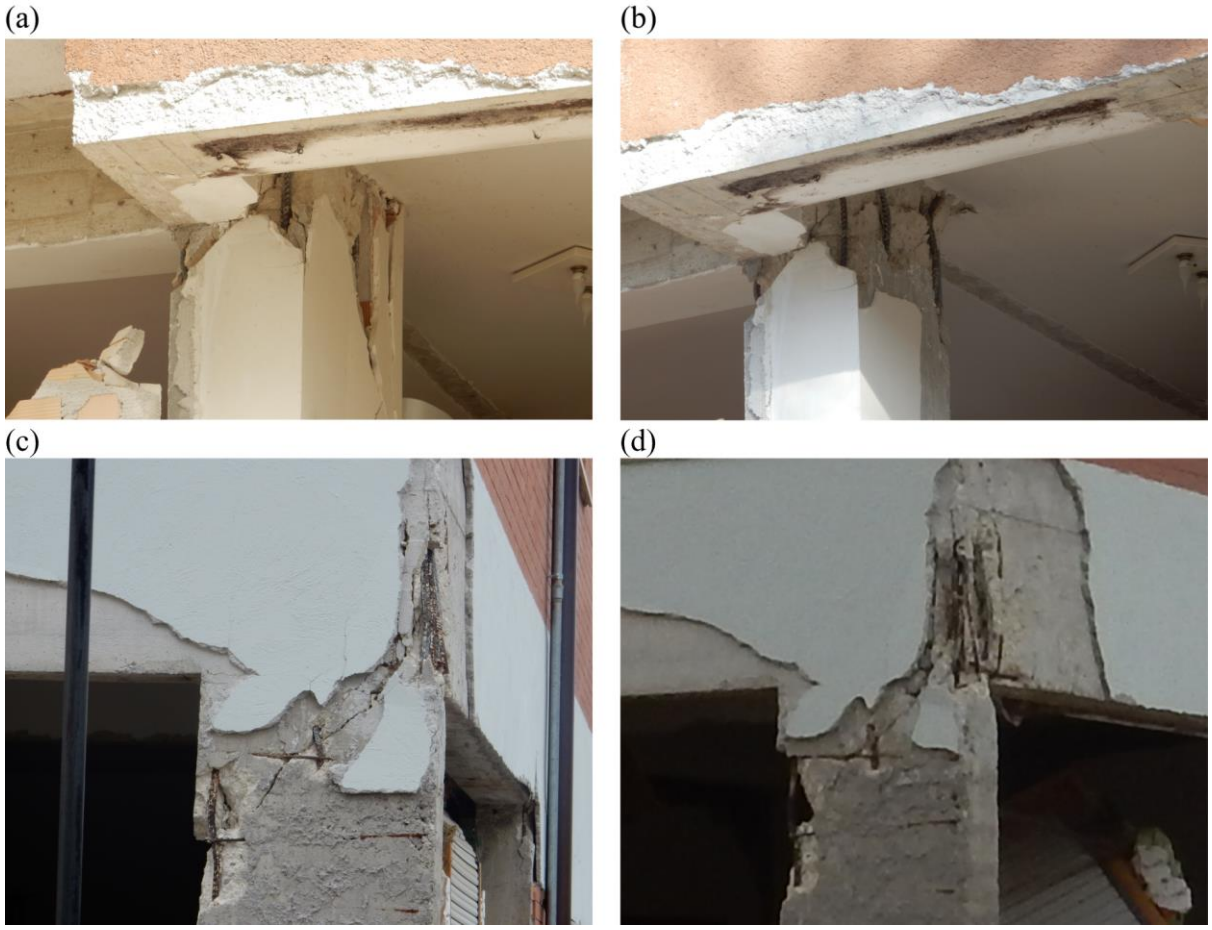

Figure 14. Beam-column joints. Concrete spalling and local bar buckling due to lack of transversal reinforcement after the 24 August event (a,c) and after the earthquake sequence (b,d).

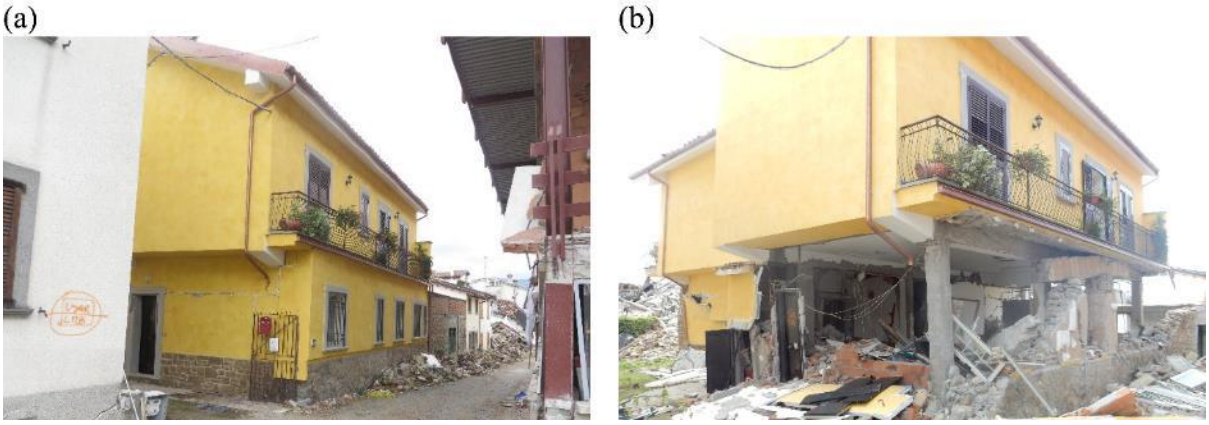

Figure 15. Irregular in plan reinforced concrete residential building. (a) limited damage after the 24 August earthquake and (b) considerable non-structural damage at ground level, failure of the infill panels and residual drift.

Figure 16. Steel residential building. (a,c) Limited damage after the 24 August earthquake and (b,d) extensive damage of the infill panels at ground level with evident residual drift after the entire sequence.

Such a steel structure consists of a basement, a ground floor, and two upper stories alongside a shorter top story that serves as a penthouse. After the 24 August event, the damage was mainly confined to the infill panels, with only small local flange instabilities observed at the top of two front columns of the ground floor. At the end of the entire seismic sequence, the building experienced permanent deformation along its longer direction, as shown in Figure 16. Such permanent deformation was localized at the second level of the building with a visible residual inter-story drift due to the relative positions of infills and openings. Preliminary finite element analyses of the building confirmed that the fundamental period of the structure is approximately equal to 0.75 sec. This was an uncoupled translational mode along the long side, which was mainly attributed to the orientation of the steel columns with their strong axes aligned with the short side of the building. Naturally, residual drift developed along the longitudinal (weak) axis. Evolution of structural damage is

also clearly seen in several characteristic masonry structures, such as the church of Sant'Agostino (Figure 17, top), the local police ("Carabinieri") station (Fig. 17, middle) and typical residential buildings (Fig. 17 bottom and Fig. 18).

Figure 17. Incremental structural damage of the church of Sant'Agostino (top), the local police station (middle) and one of the several masonry buildings collapsed after (a) the event of 24 August earthquake and (b) the entire sequence.

Figure 18. Residential **m**asonry residential building after the 24 August earthquake (a, b) and (c) after the entire sequence. Shear failure of the ground floor bearing wall leads to soft story collapse at the end of the third event.

Several general conclusions can be drawn from the damage analysis in Amatrice. Notwithstanding the clear evolution of local damage modes of reinforced concrete structures under multiple earthquake excitations, they did not experience the disproportional damage increase observed in masonry buildings. In most cases, reinforced concrete buildings showed adequate ductility and their global damage remained approximately within the same damage state that was reported in the survey that followed the first earthquake. On the contrary, masonry buildings suffered, on average, significant damage accumulation during the sequence of seismic events due to their low residual capacity and the brittle nature of their out-of-plane and shear failure modes. This led to quickly shifting from low-to-moderate Damage States (DS1-DS3) to complete collapse (DS5) and demonstrated the need for careful inspection to reliably assess their residual capacity to withstand horizontal forces during future shocks. The elevated level of damage for masonry buildings is mainly caused by the poor quality of masonry, the lack of connections between walls and the poor connection between external walls and floors, as also observed by Fiorentino et al. (2017).

Norcia

Soil conditions and building stock

Norcia is a municipality located on the border between the regions of Umbria, Marche, and Lazio. It is composed of 27 hamlets covering an area of about 274 km^2, with a population of about 4,940 inhabitants. Its core is located within the historical walls, with an altitude spanning between 590 and 630 m. The bedrock is made of sedimentary lithology units composed of unconsolidated colluvial, terraced alluvial, fluviolacustrine and fluvioglacial deposits of Pleistocene. The total number of buildings inspected in the surveyed area is 680, 98% of which are masonry residential structures. The remaining 2% is equally distributed among the reinforced concrete and other structural typologies such as steel and timber. A mere 12% of these buildings have one-story, 74% two-stories, 13% three-stories, and the remaining 1% four-stories or more. According to the last 2011 census survey (ISTAT, 2011), the 44%, 53%, and the 3% of the buildings were assessed as of optimum, good, and acceptable conservation status, respectively, a fact that reflects the overall better quality of construction compared to Accumoli and Amatrice. The majority (67%) of the buildings were built before 1919, 3% in the time period between 1946 and 1960, 3% between 1961-70, 21% between 1971-80, 4% between 1981-90, and 1% between 1990-2000.

Incremental damage observed

Figure 19 shows the structural damage levels observed during the two inspection campaigns. Following the 24 August earthquake, only a small number of buildings experienced medium or severe damage, located mainly in the historical center of the town. This good performance can be primarily attributed to two reasons. First, after the 1859 earthquake, the reconstruction of Norcia was based on a set of new practical rules of thumb prescribing a minimum wall thickness, the use of buttresses, the reduction of building height, the use of vaults only at ground floor and the mandatory presence of good wall-to-wall connections. The increased wall thickness is still visible in many structures, and in several buildings, the wall thickness varies linearly along the height of the first story. Secondly, a series of repair and strengthening works followed the 1997 Umbria-Marche event, which improved the capacity of sub-standard buildings. Such retrofits are generally not visible from outside, but confining ring-beams and cross-ties can be traced externally in many cases. Despite the adequate structural response of the buildings in Norcia during the 24 August event, a sharp increase of damage, yet not as disproportional as in the case of Amatrice, was

observed at the end of the seismic sequence, mainly in heritage construction such as churches and monasteries. The following variation of cumulative damage was reflected in the statistical distribution of the different damage states: intact buildings (DS0) were reduced from 97% after the first earthquake to 67%, which was a substantial change in structural behavior. Minor damage (DS1) also increased at the end of the entire sequence to 4% from almost 0% after the first event. The same applies to moderate damage (DS2), it increased from 1% to 24%, previously, and to DS5 increased from 0% to 3% in the first event, DS3 and DS4 remaining practically constant.

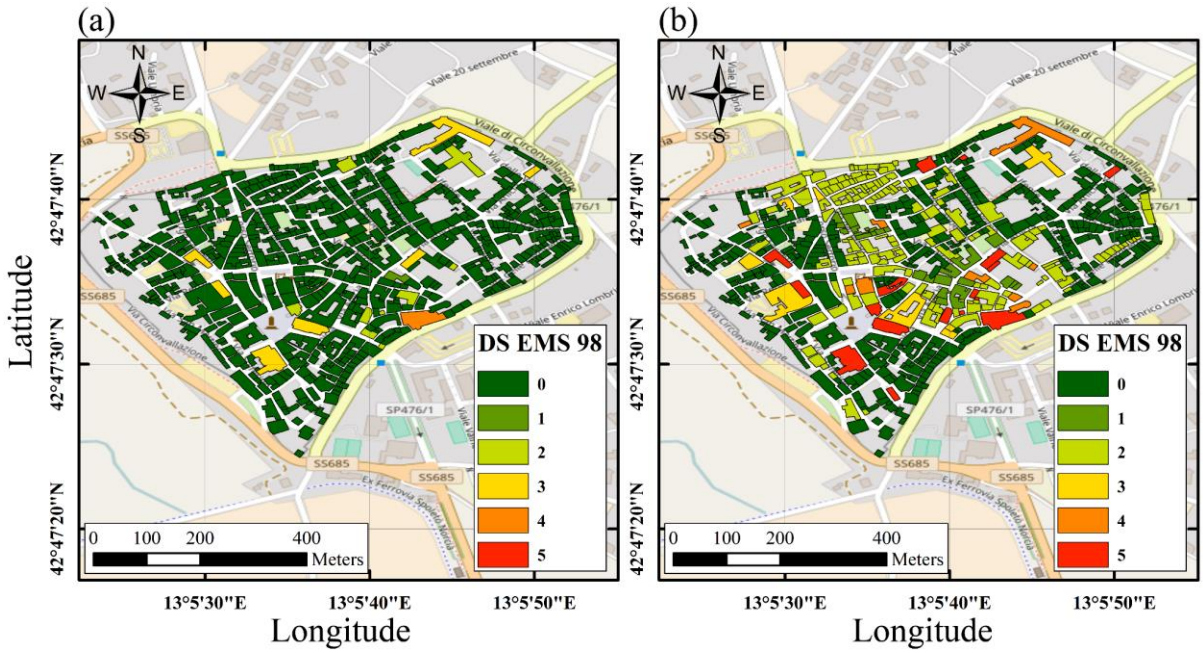

Figure 19. Damage distribution in the historical center of Norcia (a) after the 24 August event and (b) at the end of the entire seismic sequence.

Figure 20 (top) shows one of the churches that was slightly damaged by the **M**6.1 24 August seismic event but collapsed following the **M**6.5 30 October event. Many historical churches in Norcia experienced similar damage evolution, as shown for instance in Figure 20 (middle), where the out-of-plane failure of a historic monastery and the partial loss of support of the roof is depicted. Notably, the wall failure was concentrated at a level higher to that of the seismic retrofit, thus highlighting that the retrofit shall not be only localized on the ground level but also take into consideration the reduced axial load and weak diaphragm action of the masonry walls at the higher level. Figure 20 (bottom) shows two masonry residential buildings with irregular masonry construction that experienced only minor cracking during the first earthquake, but significant out-of-plane and in-plane wall failure under subsequent events.

Figure 20. Seismic damage observed in characteristic masonry buildings (a) after the 24 August earthquake and (b) at the end of the entire seismic sequence.

ON-SITE DAMAGE ASSESSMENT VERSUS NASA JPL ARIA DAMAGE PROXY MAPS

Following major natural disasters, the Advanced Rapid Imaging and Analysis (ARIA) project (ARIA, 2016a) typically publishes rapid post-disaster deformation maps. These maps are produced comparing interferometric synthetic-aperture radar (SAR) coherence maps from

before and after an extreme event (e.g., Fielding et al., 2005; Yun et al., 2011). They are usually referred to as damage proxy maps (DPMs). In the aftermath of the **M**6.5 30 October event, the ARIA team published a damage proxy map (ARIA, 2016b) for the historical center of Norcia. This DPM covers an area of 6.2-by-6.2 miles (10-by-10 kilometers), and it has been derived using the Italian Space Agency's COSMO-SkyMed Spotlight synthetic aperture radar (SAR) data acquired from an ascending orbit.

The effectiveness of the DPMs was tested for the rapid evaluation of earthquake-induced landslides and rockfalls after the 2015 **M**7.8 Gorkha Earthquake. In particular, Yun et al. (2015) showed that the extent of several observed earthquake-related instability phenomena in the Himalayas were well captured by the DPMs. Franke et al. (201x, this issue), also analyzed the effectiveness of DPMs after the **M**6.1 24 August central Italy earthquake for evaluating the spatial distribution of seismically-induced landslides and rockfalls.

The resolution of the DPM published following the **M**6.1 24 August event was too low to enable comparisons to our field observations of building damage. The DPM published following the **M**6.5 30 October event was centered on the historical center of Norcia. Given that this DPM had a relatively limited spatial extent but a high-resolution, detailed structure-by-structure comparisons of ARIA maps versus field observations were then possible. An effort was therefore made to investigate the degree of correlation between the DPM rapid imaging prediction and the actual assessment made by the members of the field mission on site.

Figure 21 shows the DPM produced for the historical center of Norcia after the **M**6.5 30 October event, that is, the end of the earthquake sequence, superimposed with 22 structures that were classified visually as completely collapsed (D5), and selected D4 structures.

By comparing the locations of these mapped structures and the damage zones from ARIA imaging, a good agreement was observed. In particular, for all structures with an assigned damage level of collapse (D5), the DPM accurately showed a concentration of red and dark red zones, representing areas in which substantial deformations occurred.

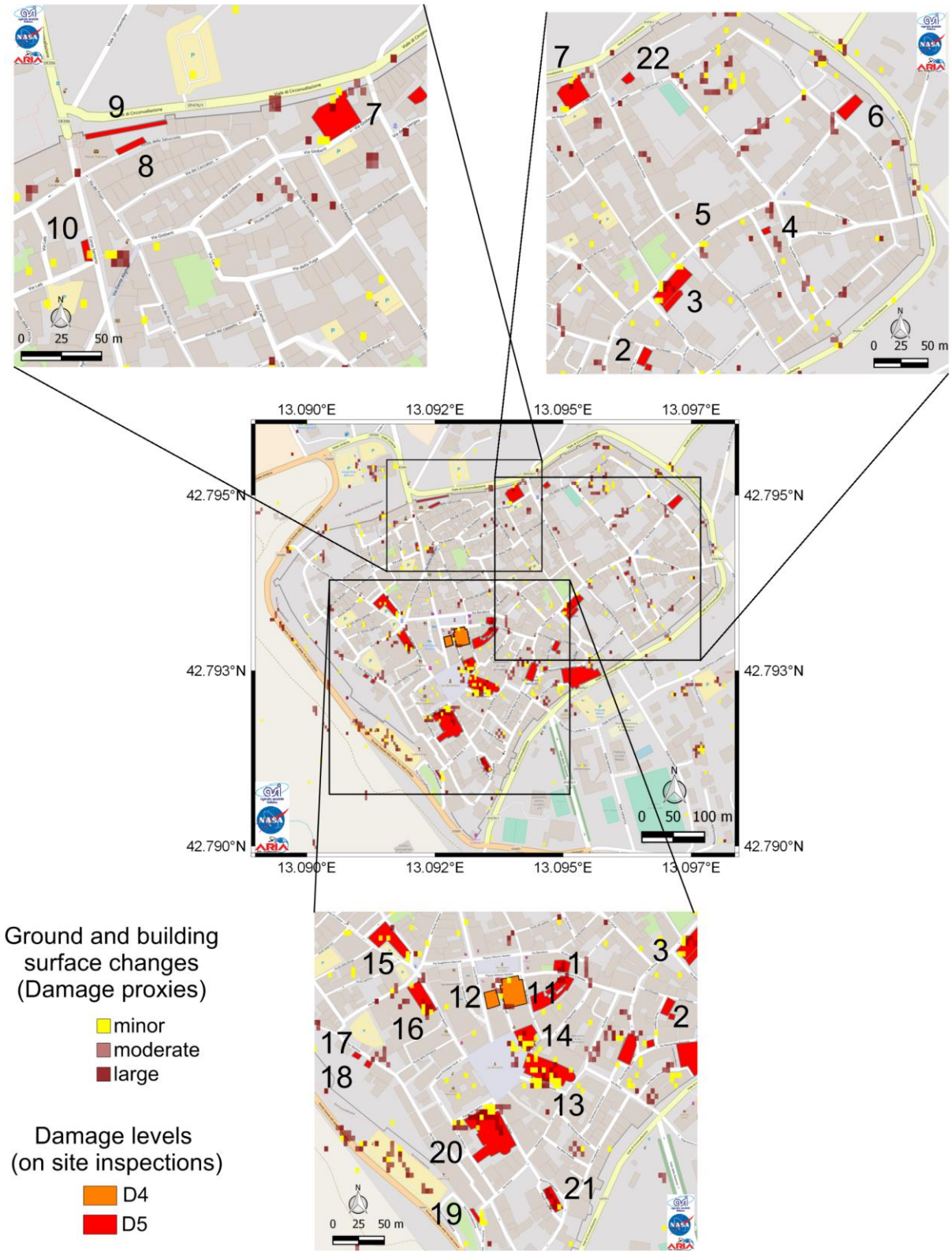

Figure 21. Damage proxy map of Norcia, along with the identification numbers of all structures with assigned damage level D5 and selected structures with assigned damage level D4, from field inspections and available high-quality on-site information and photos.

This is further documented in Figure S6, which depicts representative pictures taken during the on-site inspection that followed the 30 October, **M**6.5 earthquake event. The extent and nature of damage to each spotted building, as illustrated in Figure S6, matches well the ARIA imaging prediction highlighting the usefulness of rapid aerial assessment of seismic damage during the post-earthquake recovery period.

LESSONS LEARNED AND CONCLUSIONS

The 2016 Central Italy seismic sequence caused significant damage and loss of life. Three main events occurred between August and October 2016: (a) **M**6.1 24 August, (b) **M**5.9 26 October, and (c) **M**6.5 30 October. This paper presents the observations of two GEER field missions in the affected area with the aim to evaluate the influence of local site effects on the observed damage patterns of buildings and assess their structural performance after multiple seismic events. The first objective required an evaluation of geological and topographic conditions as well as ambient vibration measurements, where possible (H/V spectral ratios). The second objective required an extensive, building-by-building visual inspection campaign in the region and a comparative analysis of the observed damage patterns after the first main shock (**M**6.1, 24 August) and at the end of the October sequence of events.

In this process, our approach was to combine traditional reconnaissance methods (careful surveys by a team of experts on the ground) with advanced imaging and damage detection routines enabled by information and communications technologies (ICT) and geomatics approaches as well as aerial visualization with the aid of UAVs. In a number of cases, the damage was not detectable by satellite-based assessment alone, pointing to the importance of traditional on-site inspection complementing other advanced methods. For the historical center of Norcia, the damage zones from ARIA imaging (DPMs), however, compared well with damage maps obtained from on-ground surveys.

In general, the damage patterns in various municipalities and hamlets indicated a strong evidence of local site effects. Amplification of seismic waves due to stratigraphic effects in the near-surface soil deposits and due to topographic effects was the main contributor of structural damage concentration among portfolios of buildings with otherwise similar vulnerability. In addition to local site effects, the age of construction, the high-frequency content of the motions, and the variation of spectral polarization across several events further contributed to severe damage in several villages.

Another interesting observation was that the vast majority of the buildings showed a clear evolution of damage after multiple earthquake excitations irrespectively of their structural system. However, the degree of damage accumulation under repeated ground motions was different. For instance, reinforced concrete buildings did not experience disproportional damage under multiple events. These structures generally showed adequate ductility, and their damage at a systems level remained approximately constant after the first earthquake until the end of the sequence. Masonry structures, on the other hand, suffered significant damage during the first event and quite often experienced an abrupt collapse in a successive earthquake because of the rapidly reducing residual capacity and their brittle nature. Therefore, as shown in all three towns thoroughly examined (Accumoli, Amatrice, and Norcia), they quickly shifted from low to moderate damage states (D1-D2) to major damage (D4) and even collapse (D5) after the sequence of seismic events.

Local retrofit with steel ties at the corners of the upper story prevented further damage and collapse in a number of cases, particularly in Norcia where several structures had been strengthened in the last two decades. Local interventions limited on the ground level alone, however, were shown to be unsuccessful. The reduced axial load and weak diaphragm action of the masonry walls at higher levels also need to be considered during retrofit to prevent damage accumulation and possible collapse. Even though the three cases studied (Accumoli, Amatrice, and Norcia) are not directly comparable as they were exposed to different levels of ground shaking over the earthquake sequence, the overall assessment is that reinforced masonry performed significantly better than the unreinforced one and that simple measures such as ties and buttresses may be proven crucial to prevent structural collapse.

ACKNOWLEDGEMENTS

The GEER Association is supported by the U.S. National Science Foundation (NSF) through the Geotechnical Engineering Program under Grant No. CMMI-1266418. Any opinions, findings, and conclusions or recommendations expressed in this material are those of the authors and do not necessarily reflect the views of the NSF. The GEER Association is made possible by the vision and support of the NSF Geotechnical Engineering Program Directors: Dr. Richard Fragaszy and the late Dr. Cliff Astill. GEER members also donate their time, talent, and resources to collect time-sensitive field observations of the effects of extreme events.

REFERENCES

Advanced Rapid Imaging and Analysis (ARIA) – Center for Natural Hazards, 2016a. ARIA Data Share, available at https://aria-share.jpl.nasa.gov/events/ (last accessed 26 September 2017).

Advanced Rapid Imaging and Analysis (ARIA) – Center for Natural Hazards, 2016b. ARIA Data Share, available at https://aria-share.jpl.nasa.gov/events/20161030-Italy_EQ/DPM/ (last accessed 26 September 2017).

Bard, P.-Y. and J. Riepl-Thomas (2000). "Wave propagation in complex geological structures and their effects on strong ground motion." Wave motion in earthquake eng: 37-95.

Boore, D. M., Stewart, J. P., Seyhan, E., Atkinson, G. M., 2014. NGA-West 2 equations for predicting PGA, PGV, and 5%-damped PSA for shallow crustal earthquakes. *Earthquake Spectra*, **30**, 1057-1085.

Brambati, A., E. Faccioli, G. Carulli, F. Cucchi, R. Onofri, S. Stefanini and F. Ulcigrai (1980). "Studio di microzonazione sismica dell'area di Tarcento (Friuli)." CLUET, Trieste.

BYU-PRISM, 2016. 3D model gallery – 2016 Central Italy Earthquakes, available at http://prismweb.groups.et.byu.net/gallery2/2016%20Central%20Italy%20Earthquakes/ (last accessed 26 September 2017).

Campbell, K. W., and Bozorgnia, Y., 2014. NGA-West2 ground motion model for the average horizontal components of PGA, PGV, and 5% damped linear acceleration response spectra. *Earthquake Spectra*, **30**, 1087-1115.

CEN, European Committee for Standardization, (2004). EN 1998-1 Eurocode 8 (2004): Design of structures for earthquake resistance – Part 1: General rules, seismic actions and rules for buildings. Brussels, BE.

Center for Seismic Microzonation and its applications – CentroMS, 2016. Terremoto Centro Italia, available at https://www.centromicrozonazionesismica.it/it/attivita/terremoto-centro-italia (last accessed 26 September 2017).

Chiou, B. S. J., and Youngs, R. R., 2014. Update of the Chiou and Youngs NGA model for the average horizontal component of peak ground motion and response spectra. *Earthquake Spectra*, **30**, 1117-1153.

Copernicus, 2016. Emergency management service (EMS) mapping, EMSR177: Earthquake in Central Italy, available at http://emergency.copernicus.eu/mapping/list-of-components/EMSR177/ALL/EMSR177_20AMATRICEAERIAL (last accessed 26 September 2017).

Cramer, C. H., 2003. Site-specific seismic-hazard analysis that is completely probabilistic, *Bull. Seismol. Soc. Am.*, **93**, 1841–1846.

Faccioli, E., Vanini, M., and Frassine, L. (2002). Complex site effects in earthquake ground motion, including topography. 12th European Conference on Earthquake Engineering.

Fiorentino, G., Forte, A., Pagano, E., Sabetta, F., Baggio, C., Lavorato, D., ... & Santini, S. (2017). "Damage patterns in the town of Amatrice after August 24th 2016 Central Italy earthquakes." Bulletin of Earthquake Engineering, 1-25. https://doi.org/10.1007/s10518-017-0254-z.

Franke et al., 201x. A multi-scale reconnaissance approach to documenting landslides following the 2016 Central Italy earthquakes. *Earthquake Spectra*, in review.

Frankel, A., and Vidale, J., 1992. A three-dimensional simulation of seismic waves in the Santa Clara Valley, California, from a Loma Prieta aftershock, Bull. Seismol. Soc. Am. 82, 2045–2074.

Galadini et al., 201x. Tectonic setting of 2016-2017 Central Italy event sequence and observed source characteristics. *Earthquake Spectra*, in review.

Gallipoli, M., M. Bianca, M. Mucciarelli, S. Parolai and M. Picozzi (2013). "Topographic versus stratigraphic amplification: mismatch between code provisions and observations during the L'Aquila (Italy, 2009) sequence." Bulletin of Earthquake Engineering 11(5): 1325-1336.

GEER, 2016. Engineering Reconnaissance of the 24 August 2016 Central Italy Earthquake. Version 2, Zimmaro P. and Stewart J.P. (editors), Geotechnical Extreme Events Reconnaissance Association Report No. GEER-050B. doi: 10.18118/G61S3Z.

GEER, 2017. Engineering Reconnaissance following the October 2016 Central Italy Earthquakes - Version 2, Zimmaro P. and Stewart J.P. (editors), Geotechnical Extreme Events Reconnaissance Association Report No. GEER-050D. doi:10.18118/G6HS39.

Goulet, C. A., and Stewart, J. P., 2009. Pitfalls of deterministic application of nonlinear site factors in probabilistic assessment of ground motions, *Earthquake Spectra*, **25**, 541–555.

ISTAT (Istituto Nazionale di statistica), 2011. Censimento popolazione e abitazioni 2011, available at http://dati-censimentopopolazione.istat.it/Index.aspx (last accessed 26 September 2017).

Jayaram, N., and Baker, J. W., 2009. Correlation model for spatially distributed ground-motion intensities, *Earthquake Engineering and Structural Dynamics*, **38**, 1687–1708.

Marsan, P., G. Milana, A. Pugliese and T. Sanò (2000). Local amplification effects recorded by a local strong motion network during the 1997 Umbria-Marche earthquake. Proceedings of the 12th world conference on earthquake engineering, New Zealand.

Ministry of Public Works - Italy, 1996. Norme tecniche per le costruzioni in zone sismiche, Decree of the Minister of Public Works, 5 February 1996, Gazzetta Ufficiale della Repubblica Italiana No. 29, Rome (in Italian).

Ministry of the environment (Ministero dell'Ambiente), 2014. Geoportale nazionale, available at http://www.pcn.minambiente.it/GN (last accessed 26 September 2017).

Ministry of the Infrastructures - Italy, 2008. Norme tecniche per le costruzioni, Decree of the Minister of the Infrastructures, 14 January 2008, Gazzetta Ufficiale della Repubblica Italiana No. 29, Rome (in Italian).

Olsen, K.B., and Schuster, G.T., 1995. Causes of low-frequency ground motion amplification in the Salt Lake Basin: the case of the vertically-incident P wave, Geophys. J. Int. 122, 1045–1061.

Pagliaroli, A., G. Lanzo and B. D'Elia (2011). "Numerical evaluation of topographic effects at the Nicastro ridge in Southern Italy." Journal of earthquake Engineering 15(3): 404-432.

Paolucci, R. (2002). "Amplification of earthquake ground motion by steep topographic irregularities." Earthquake Engineering & Structural Dynamics 31(10): 1831-1853.

Regione Marche, 2014. Microzonazione sismica del Comune di Arquata del Tronto. Attuazione art. 11 legge n.77/2009. OCDPC n. 52/2013. Approvato dalla Regione Marche.

Regione Marche, 2015. Microzonazione sismica del Comune di Montegallo. Attuazione art. 11 legge n.77/2009. OCDPC n. 171/2014. Approvato dalla Regione Marche.

Regione Marche (2012). Microzonazione sismica del Comune di Visso. Attuazione art. 11 legge n.77/2009. OPCM n. 3907/2010. Approvato dalla Regione Marche.

Roesset, J. M. (1970). Fundamentals of soil amplification, Massachusetts Inst. of Tech., Cambridge.

Rovelli, A., B. Caserta, F. Palomba, G. Bellucci, G. Cultrera, F. Marra, G. Mele and S. Donati (1998). Amplification of ground motion due to topography and sedimentary filling in the Nocera Umbra area (Central Italy). Proceedings of the Second International Symposium on The Effects of Surface Geology on Seismic Motion.

Sanchez-Sesma, F. J. (1987). "Site effects on strong ground motion." Soil Dynamics and Earthquake Engineering 6(2): 124-132.

Sarconi, M. (1784). Istoria de fenomeni del tremoto avvenuto delle Calabrie, e nel Valdemone nell'anno 1783, Campo.

Seed, H., M. Romo, J. Sun, A. Jaime and J. Lysmer (1988). "The Mexico earthquake of September 19, 1985—Relationships between soil conditions and earthquake ground motions." Earthquake Spectra 4(4): 687-729.

Sextos, A., 2016. Amatrice post-earthquake assessment, available at https://www.youtube.com/watch?v=djF5fkUrYkk (last accessed 26 September 2017).

Siro, L. (1982). Southern Italy November 23, 1980 earthquake. Proceedings of the seventh European conference on earthquake engineering, Athens, Greece.

Stewart, J. P., Afshari, K., and Goulet C. A., 2017. Non-ergodic site response in seismic hazard analysis, Earthq. Spectra. DOI: http://dx.doi.org/10.1193/081716EQS135M.

Stewart, J. P., K. Afshari and Y. M. Hashash (2014). "Guidelines for performing hazard-consistent one-dimensional ground response analysis for ground motion prediction." PEER Rep 16.Regione Lazio, 2016. Microzonazione sismica del Comune di Amatrice. Attuazione art. 11 legge n.77/2009. In corso di approvazione da parte del DPC ai sensi OPCM 4007/2012.

Zimmaro et al., 201x. Strong Ground Motion Characteristics from 2016 Central Italy Earthquake Sequence. *Earthquake Spectra*, in review.

Zimmaro P., Kwak D.Y., Stewart J.P., Brandenberg S.J., Balakrishnan A., Jongejan R., Ausilio E., Dente G., Xie J., Mikami A. (2017). Procedures from international guidelines for assessing seismic risk to flood control levees. *Earthquake Spectra*, **33**, 1191-1218.

Zimmaro, P., and Stewart, J. P., 2017. Site-specific seismic hazard analysis for Calabrian dam site using regionally customized seismic source and ground motion models. *Soil Dynamics and Earthquake Engineering*, **94**, 179-192.

Stewart, J. P., Lanzo, G., Pagliaroli, A., Scasserra, G., Di Capua, G., Peppoloni, S., Darragh, R. B., and Gregor, M., 2012. Ground Motion Recordings from the Mw 6.3 2009 L'Aquila Earthquake in Italy and their Engineering Implications. *Earthquake Spectra*, **28**, 317-345.